

PROPERTY TAILORABILITY FOR ADVANCED CVI SILICON CARBIDE COMPOSITES FOR FUSION—Y. Katoh, T. Nozawa, and L. L. Snead (Oak Ridge National Laboratory), T. Hinoki and A. Kohyama (Kyoto University)

OBJECTIVE

The objective of this work is to determine the tailorability of anisotropic thermomechanical properties for chemically vapor-infiltrated (CVI) SiC/SiC composites after neutron irradiation.

SUMMARY

Chemically vapor infiltrated (CVI) silicon carbide (SiC) matrix composites with uni-directional and various two- and three-dimensional reinforcements with near-stoichiometric SiC fibers or SiC/graphite hybrid fabrics were produced and evaluated for tensile, thermal and electrical properties. The parallel-serial approach models of these properties reasonably explained the experimental results. The experimental data and the model-based analysis suggested that: (1) the strength properties are determined primarily by the volume fraction of longitudinal fibers, approximately following the theory that assumes global load sharing, (2) presence of the axial fiber tows is the key factor in providing high thermal conductivity as it is determined by the significant contributions from the axial fibers (when present), matrix within and surrounding the axial fiber tows, and the remaining constituents of the composite, (3) among the composite systems studied, the maximum and minimum post-irradiation through-thickness conductivity observed were 10–15 W/m-K at 800–1000°C for 3D architecture and < 5 W/m-K at < 800°C for 2D architecture, respectively, and (4) the orthogonal 3D configurations of $x:y:z = 1:1:0.2$ – $1:1:0.5$ will provide the highest post-irradiation resistance to thermal stress due to through-thickness heat flow.

PROGRESS AND STATUS

Introduction

Silicon carbide (SiC) is a unique material that retains its strength and chemical stability at elevated temperatures and under intense neutron irradiation [1]. Additionally, SiC provides safety features when applied to fusion nuclear systems due to its low activation / low decay heat characteristics [2]. SiC fiber-reinforced SiC-matrix composites (SiC/SiC composites), which add mechanical damage tolerance to inherently brittle monolithic SiC, are thus promising candidates for fusion blanket / first wall structures [3], and flow channel inserts [4]. Due to the complex role and design diversity of the breeding blankets of fusion reactors, the proposed application of SiC/SiC composites to various blanket designs demands a wide range of material properties [5]. Mechanical strength and thermal and electrical conductivity are the properties of primary concern for fusion blanket applications, and they can be anisotropically tailored in fibrous composites.

The objectives of this work are to determine the tailorability of anisotropic thermomechanical properties for chemically vapor-infiltrated (CVI) SiC/SiC composites and the trade-off between the mechanical and thermal properties. For these purposes, CVI SiC-matrix composites were fabricated employing the uni-directional (UD), common two-dimensional (2D), and three-dimensional (3D) reinforcements by near-stoichiometric SiC fibers and their mechanical and thermal / electrical transport properties were evaluated. The measured properties were analyzed using theoretical models and the influence of neutron irradiation on temperature dependent composite properties was predicted.

Experimental Procedure

Materials

Various composites were produced through an isothermal / isobaric CVI process [6]; three of them were in uni-directional (UD) architecture, four in 2D fabric lay-up architecture, and three in orthogonal 3D architecture, as listed in Table 1. All the 2D composites employed [0°/90°] lay-up of the plain-weave (PW) or 5-harness satin-weave (5H SW) fabrics. The PW and SW are the two types of architectures which have been extensively studied for 2D SiC/SiC composites, whereas the orthogonal 3D is not only the most common but also the most easily property-tailorable 3D architecture.

Table 1. List of materials studied

Material ID	Fiber	Reinforcement Architecture	Fiber Volume Fractions [%]		Fiber/Matrix Interphase	Mass Density [g/cm ³]	Porosity [%]
			x or y	z			
UD ML	HNLS ¹	UD ⁴	38	0	ML ^{7,8}	2.3	26
UD PyC1	HNLS	UD	29	0	PyC ⁹ (500nm)	2.6	19
UD PyC2	HNLS	UD	29	0	PyC(800nm)	2.5	19
PW TySA	TySA ²	2D PW ⁵ [0°/90°]	20	0	PyC(150nm)	2.5	20
PW HNLS	HNLS	2D PW [0°/90°]	20	0	ML ^{7,8}	2.6	18
SW HNLS	HNLS	5HSW ⁶ [0°/90°]	22	0	PyC(150nm)	2.5	19
Hybrid 2D	TySA/P120S ³	2D Hybrid PW ^{5,7} [0°/90°]	8/15	0	PyC(150nm)	2.3	19
3D 1:1:1	TySA	3D Orthogonal, x:y:z =1:1:1	15	15	PyC(150nm)	2.8	11
3D 1:1:4	TySA	3D Orthogonal, x:y:z =1:1:4	7.5	30	PyC(150nm)	2.8	10
Hybrid 3D	TySA/P120S	3D Hybrid ⁷ , x:y:z =1:1:1.8	12	21	PyC(150nm)	2.2	25

¹Hi-Nicalon™ Type S, ²Tyranno™-SA3, ³Thornel P-120S, ⁴Uni-directional, ⁵Plain-weave, ⁶5-harness satin-weave, ⁷See text, ⁸(PyC/SiC) multi-layered interphase, ⁹Pyrolytic carbon

The composites were reinforced primarily by near-stoichiometric SiC fibers, namely Tyranno™-SA3 (Ube Industries, Ltd., Ube, Japan) or Hi-Nicalon™ Type-S (Nippon Carbon Co., Tokyo, Japan). The Hybrid 3D composite incorporated Thornel™ P-120S pitch-based graphite fibers (Cytec Engineered Materials, Inc., Anaheim, CA) in the through-thickness or 'z' direction, whereas it used Tyranno™-SA3 for the in-plane ('x' and 'y' directions) reinforcement. The Hybrid 2D-PW composite was made from interlaced hybrid fabrics, in which the Tyranno™-SA3 and P-120S strands were woven alternatively for both x and y tows. A single-layered pyrolytic carbon (PyC) interphase was applied to each of the PyC-interphase composites. A multi-layered (ML) interphase, in which five thin PyC layers of 20nm each were separated by the SiC layers of 100nm thick, was deposited only onto the UD ML and 2D-PW Hi-Nicalon™ Type-S composite [7]. The mean porosities for the 2D composites estimated from densitometry were ~ 20%, whereas those for the 3D composites varied in a range of 10–25%. The optical micrographs of polished cross-sections for these composites are shown in Fig. 1.

Property Evaluation

Mechanical properties were evaluated by the tensile test using rectangular bar specimens, in which the tensile axis was parallel to the x direction. The specimen dimensions were 40mm (length) x 4mm (width) x 2.3mm (thickness) for 2D and 50mm x 6mm x 2.5mm for 3D composites. The tensile test was conducted at room temperature following the general guidelines of ASTM C1275. The strain was measured by averaging the readings of strain gauges attached to both faces of the specimens.

Thermal diffusivity measurement was performed using a xenon lamp flash technique. Thermal conductivity was then calculated using the measured composite mass density and the composite specific heat estimated by the rule of mixture using the literature values for the constituents' specific heats.

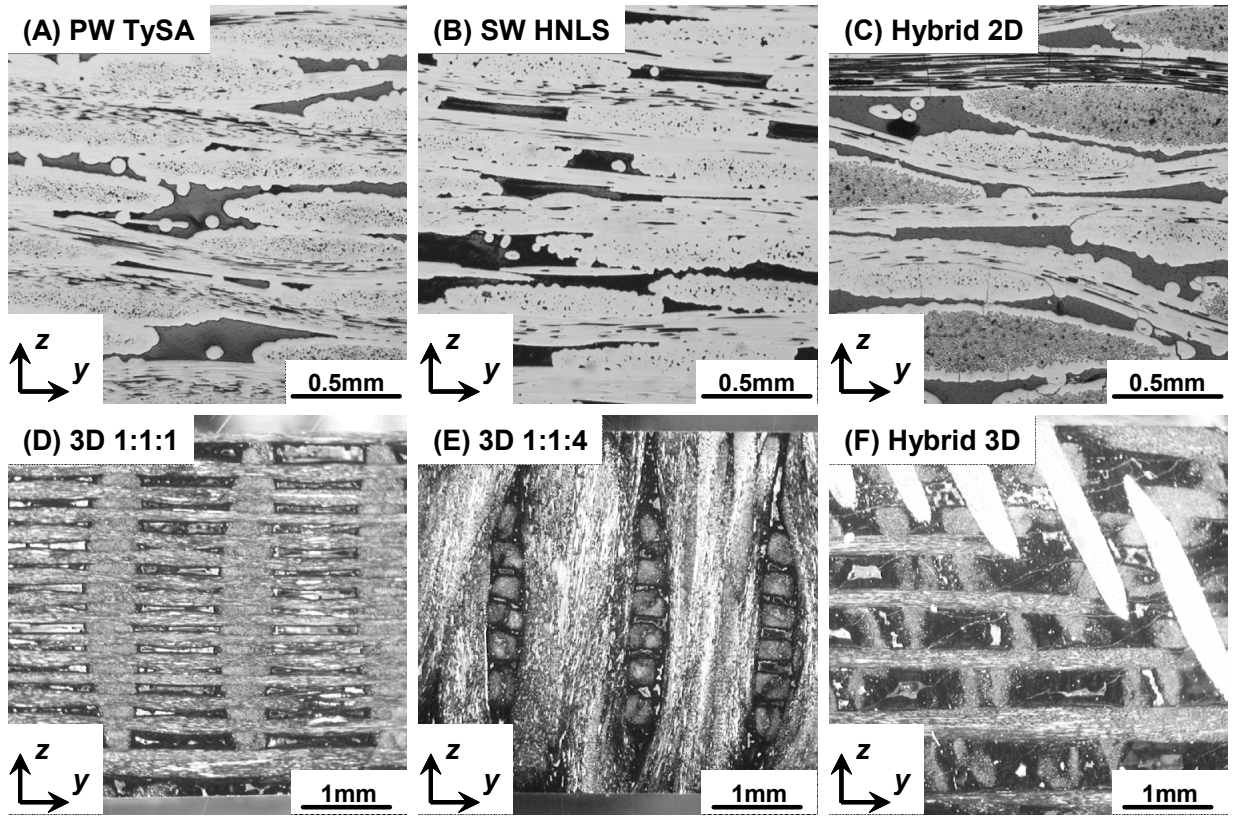


Fig. 1. Optical images of the polished y (horizontal) - z (vertical) cross-sections of the 2D and 3D composites, showing the transverse cross-sections of the x -fiber tows (all) and longitudinal cross-sections of y - (A-D, F) and z - (D-F) fiber tows. In the Hybrid 2D composite (C), the graphite fibers appear in a darker contrast, and the matrix micro-cracks due to a mismatch in thermal expansion are seen. In the Hybrid 3D composite (F), the graphite z -fibers appear inclined and in a brighter contrast.

Model Analysis

The composite elastic moduli and thermal conductivities were analyzed based on the Parallel-Serial Approach (PSA) model proposed by Ishikawa et al. [8]. In this model, modulus and conductivity of the unit cell (shown in Fig. 2) in x , y , or z direction are calculated using a simple rule of mixture for multiple parallel and serial components, based on anisotropic moduli and conductivities of the 'mini-composites' (single tow + interphase + surrounding matrix) and the inter-tow matrix incorporating large pores. As for the 2D composites, the unit structure was approximated by the orthogonal 2D architecture as shown in Fig. 2A, incorporating three types of matrix elements. The Type-I and Type-II matrices are the inter-tow matrices, which include pores arising from the cross-over of tows and the fabric mesh, respectively, and a Type-III inter-laminar matrix, which includes large planar inter-laminar pores. Each inter-tow or inter-laminar matrix element was given anisotropic load/heat/electricity transfer efficiency factors, which are determined by a volume fraction and a shape factor of pores in it. For example, the through-thickness property X_z for the orthogonal 3D architecture is calculated as follows:

$$X_z = \frac{X_I X_{II}}{h_2 X_I + h_1 X_{II}} \quad (1)$$

and:

$$X_I = cdX_L + ad\varepsilon_z X_m + bX_T \quad (2a)$$

$$X_{II} = cdX_L + cb\varepsilon_z X_m + aX_T \quad (2b)$$

$$X_L = fX_f + iX_i + mX_m \quad (3a)$$

$$X_T = \frac{X_f X_i X_m}{fX_i X_m + iX_f X_m + mX_f X_i} \quad (3b)$$

where X_I and X_{II} are the moduli/conductivities of layers I and II, X_L and X_T are the longitudinal and transverse moduli/conductivities of the mini-composite element, X_f , X_i and X_m are the intrinsic moduli/conductivities of fiber, interphase and matrix, respectively, $h_1 + h_2 = a + b = c + d = 1$ (see Fig. 2), and f , i , and m denote the volume fraction of fiber, interphase and matrix in the mini-composite element, respectively. ε_z is the matrix conduction efficiency factor in z direction and given by:

$$\varepsilon_z = (1-p)^\beta; \quad \beta = \frac{1 - \cos^2 \alpha}{1-F} + \frac{\cos^2 \alpha}{2F} \quad (4)$$

where p is porosity within the element, α is the angle between z and axis of symmetry for a planar pore, and F is the pore shape factor ($F = 1/3$ for sphere and $F \rightarrow 0$ for lamella) [9].

The constituent properties used in the analysis are summarized in Table 2. The geometric parameters were given based on the ceramographic examination. The matrix porosity parameters were used as adjustable parameters, although the results were generally insensitive to ε_z , except for the effect of ε_z for Type-III matrix on through-thickness properties of 2D composites.

The effects of elevated temperatures and neutron irradiation on thermal conductivity were treated by modifying the thermal conductivity of each constituent in accordance with the linear thermal resistance model proposed by Snead et al. [10].

Results and Discussion

Mechanical Properties

The results of tensile tests are summarized in Table 3. The 2D SiC/SiC composites exhibited ultimate tensile strength (UTS) and proportional limit stress (PLS) similar to the typical SiC/SiC composites evaluated previously [11,12]. The 3D and Hybrid 2D composites exhibited significantly lower strength than the 2D SiC fiber composites. Under the assumed condition of global load sharing, where the intact longitudinal fibers carry the load equally, the UTS is proportional to the product of longitudinal fiber volume fraction (V_f) and characteristic fiber strength (σ_c):

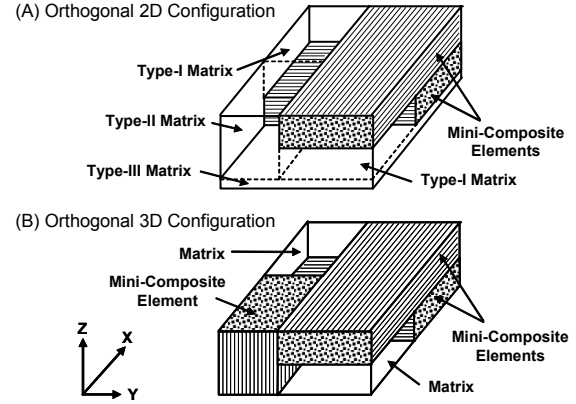


Fig. 2. Configuration of unit cells for orthogonal 2D (A) and 3D (B) architectures for modeling the anisotropic modulus and transport properties of woven fabric CVI composites by the Parallel-Serial Approach.

Table 2. Constituent properties and geometrical parameters used in calculation

	Tyranno™-SA3	Hi-Nicalon™ Type S	P-120S	Matrix SiC	PyC Interphase
Elastic modulus [GPa]	420	400	840	450	12
Thermal conductivity (20°C) [W/m-K]	64	18	640	70	5
Electrical conductivity (20°C) [S/m]	5	2	-	10	3x10 ⁴

Table 3. Summary of experimentally measured (“Meas.”) and model-calculated (“Model”) properties. Numbers in parentheses are standard deviations.

Material ID	UTS [MPa]	PLS [MPa]	Modulus [GPa]		Thermal Conductivity [W/m-K]				Electrical Conductivity [S/m]	
					Through-thickness		In-plane		In-Plane	
					Meas.	Model	Meas.	Model	Meas.	Model
UD ML	249(18)	249(18)	306(62)	321	n/m	-	n/m	-	200	208
UD PyC1	442(120)	339(12)	307(8)	338	n/m	-	n/m	-	900	1160
UD PyC2	319(56)	268(37)	306(51)	330	n/m	-	n/m	-	1700	1690
PW TySA	199(2)	103(21)	273(23)	272	18.9(0.3)	20.9	47.8(1.3)	48.5	n/m	-
PW HNLS	n/m	n/m	n/m	286	18.6	16.1	n/m	33.9	n/m	-
SW HNLS	226(50)	101(9)	244(6)	303	18.1(0.3)	15.3	34.7(1.3)	32.5	n/m	-
Hybrid 2D	94(28)	8(1)	138(28)	311	n/m	-	n/m	-	n/m	-
3D 1:1:1	102	53	227	225	46.1(0.9)	46.3	47.4(1.0)	44.1	n/m	-
3D 1:1:4	59(13)	35(2)	224(5)	248	58.2(1.8)	55.1	46.2(1.4)	46.1	n/m	-
Hybrid 3D	98(3)	47(1)	95(10)	248	53.0(13.5)	116.3	32.6(0.5)	31.2	n/m	-

*n/m: not measured

$$\sigma_u = V_f \sigma_c \left(\frac{2}{m+2} \right)^{1/(m+1)} \cdot \frac{m+1}{m+2} \quad (5)$$

where m is the Weibull modulus for individual fiber strength [13]. On the other hand, the matrix cracking stress (σ_{mc}), which approximately corresponds to the PLS, is given by:

$$\sigma_{mc} = \left[\frac{6\tau\gamma_m}{r} \cdot \frac{V_f^2 E_f E_c^2}{(1-V_f)E_m^2} \right]^{1/3} \quad (6)$$

where τ is the interfacial sliding stress, γ_m is the matrix fracture energy, r is the fiber radius, E_f , E_m , and E_c are the Young's moduli of fiber, matrix, and composite, respectively [13]. Equation 6 gives a monotonic and nearly linear relationship between σ_{mc} and V_f in the V_f range of interest. Such relationships are seen in Fig. 3, where the measured UTS and PLS are plotted against the longitudinal fiber volume fraction. Fitted lines based on Eqs. 5 and 6 are drawn together. The lower UTS for the 3D SiC/SiC composites is attributed to the reduced fiber strength due to the additional heat treatment to the 3D woven fabric. As shown in Table 3, the tensile modulus calculated using the model yielded a good agreement with the experimental result except for the cases of hybrid 2D and 3D composites. The reason for exceptionally low UTS and modulus for the hybrid composites is introduction of process-induced matrix microcracks (shown in Figs. 1C and F) due to the mismatch in coefficients of thermal expansion (CTE) between the graphite fibers and the matrices.

Thermal Conductivity

Thermal conductivity measured along the in-plane and through-thickness directions at room temperature is summarized in Table 3. The Hybrid 2D composite underwent delamination during processing and, therefore, was not subjected to thermal conductivity measurement. The data are also plotted in Fig. 4 as a function of the estimated contribution from the fibers along the heat transport axis to the composite thermal conductivity. The in-plane fiber contribution to through-thickness thermal conductivity in the 2D composite systems is due to the through-thickness component of the wavy fiber tows in 2D woven fabrics. The linear fit indicates the slope of slightly higher than unity and intersects the vertical axis at ~ 35 W/m-K, in contrast to the 15–20 W/m-K of through-thickness thermal conductivity for the 2D composites. This implies a significant contribution of the matrix within and surrounding the axial fiber tows, in addition to the contribution from the axial fibers themselves, to the composite thermal conductivity. Therefore, the presence of the axial fiber tows is the key factor that enables a large heat conductance. In other words, the large planar matrix pores distinctive to the 2D laminate composites are effective in lowering the through-thickness heat transport.

The model-prediction showed a good agreement between the calculated and experimental thermal conductivity in both the in-plane and through-thickness directions, as shown in Table 3. The geometric parameters used for thermal conductivity are identical with those used for the elastic modulus calculation. It was assumed that these results validate the applicability of this approach to the approximate estimation of various transport properties in the present composite systems.

In Fig. 5, the calculated temperature dependence of thermal conductivity for selected composites is presented along with experimental data [14]. For this calculation, linearly temperature dependent reciprocal thermal diffusivity was assumed for both matrix and fibers, based on the thermal conductivity data for chemically vapor-deposited SiC [14], and the coefficient of thermal resistance was adjusted to fit the experimental data in Fig. 5.

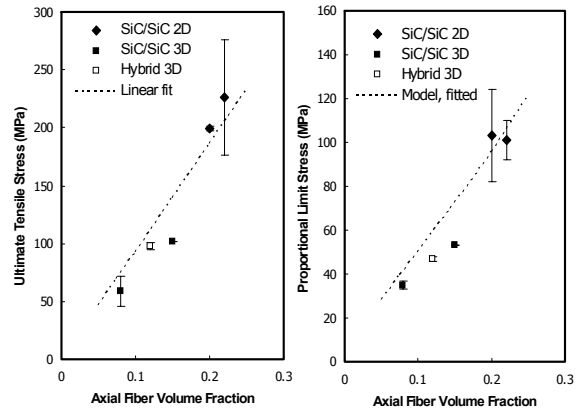


Fig. 3. The influence of fiber volume fraction along the tensile axis on the ultimate tensile stress and proportional limit stress. Error bars indicate the standard deviation. The low strength for Hybrid 2D composite is due to process-induced extensive matrix cracking.

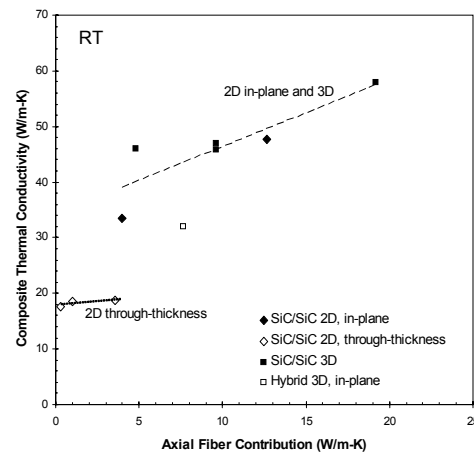


Fig. 4. Effect of heat conduction through axial fibers on composite thermal conductivity at room temperature. The dotted line represents a linear fit to data points for SiC/SiC composites in one of the fiber directions.

Neutron irradiation is known to further increase thermal resistance for SiC, which initially increase with fluence and tends to saturate by a few dpa of neutron exposure. The saturated defect thermal resistance is linearly dependent on the irradiation temperature at 300–800°C [15] and the data could be fitted to the equation below:

$$\frac{1}{K_{rd}} = 0.119 - 1.13 \times 10^{-4} T(^{\circ}\text{C}) \quad (7)$$

Figure 6 presents the post-irradiation thermal conductivity at the irradiation temperature calculated using Eq. 7. The positive temperature dependence of the post-irradiation thermal conductivity is due to the strong contribution from the defect thermal resistance, in contrast to the negative temperature dependence for the non-irradiated materials. The model prediction suggests that, when through-thickness fibers are incorporated in CVI SiC-matrix composites, the post-irradiation through-thickness thermal conductivity of 10–15 W/m-K is feasible for high-heat flux applications at 800–1000°C, which is the temperature range of primary interest for power reactor design studies [5]. Meanwhile, 2D laminated composites are more appropriate when the through-thickness thermal conductivity < 5 W/m-K is desired under irradiation at < 800°C, which is of interest for the flow channel insert application [4]. Substantial increase or reduction in through-thickness thermal conductivity from these upper or lower limits will require the incorporation of a heat conductive or thermally insulating medium within the composites [16].

Optimizing the 3D Configuration

For high through-thickness heat flux applications such as blanket first walls, thermal stress arising from the temperature gradient across the wall thickness will be a major design issue that limits the operating condition of specific systems [5]. The general resistance of materials to thermal stress is conveniently indexed by a thermal stress figure of merit (M) [17]:

$$M = \frac{\sigma_a K_{th} (1 - \nu)}{\alpha E} \quad (7)$$

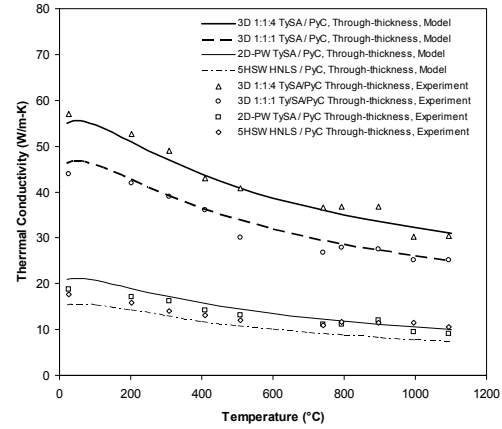


Fig. 5. Temperature-dependent thermal conductivity of various CVI SiC/SiC composites: comparison of model-prediction and experimental data.

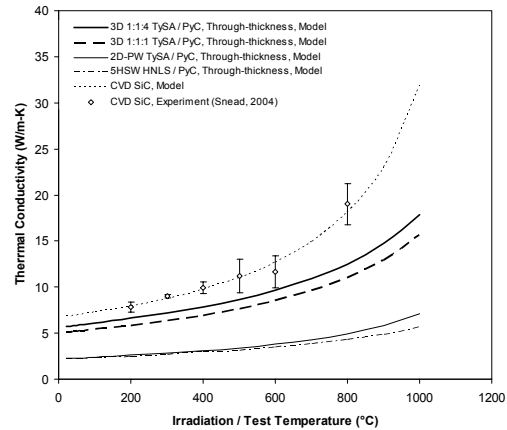


Fig. 6. Post-irradiation thermal conductivity of CVI SiC/SiC composites as a function of temperature predicted by the model. The temperature at which thermal conductivity was calculated is equal to the irradiation temperature.

using the allowable design stress (σ_a), through-thickness thermal conductivity (K_{th}), Poisson's ratio (ν), coefficient of in-plane thermal expansion (α), and in-plane elastic modulus (E). In Fig. 7, the predicted influence of z-fiber fraction in 1:1:z configuration on the through-thickness thermal conductivity, tensile strength properties, and the thermal stress figure of merit for 3D SiC/SiC composites is presented. The PLS was used as the allowable stress. The influences of elevated temperature and neutron irradiation on the mechanical properties were neglected since they should not greatly alter the z-fiber fraction dependence and the magnitude of the influence was reported to be minor [3,18]. The result indicates that the highest resistance to thermal stress occurs at 1:1:0.5–1.0 at room temperature before irradiation, but the z-fiber fraction that gives the peak M values shifts to 1:1:0.2–0.5 at elevated temperatures and/or after irradiation. Also, the M value appeared insensitive to the z-fiber fraction in this range.

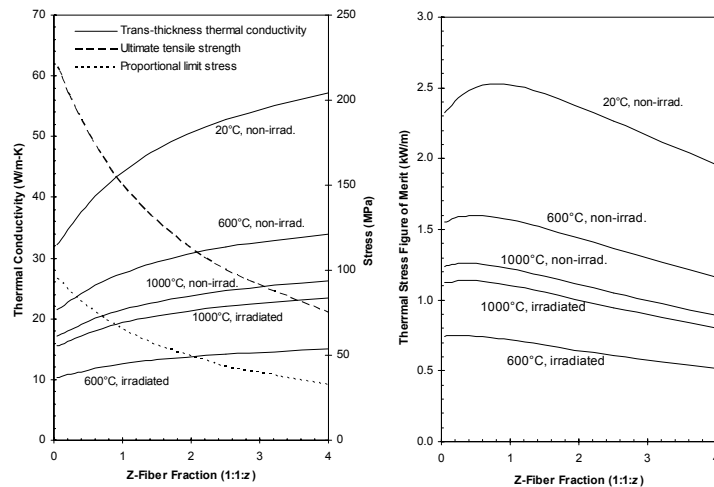


Fig. 7. The predicted influence of z-fiber volume fraction in 1:1:z orthogonal 3D configuration on non-irradiated and irradiated through-thickness thermal conductivity, in-plane tensile properties, and thermal stress figure of merit for Tyranno™-SA CVI SiC-matrix composites.

Acknowledgement

Thanks are extended to Drs. H-T. Lin, S. J. Zinkle, and R. E. Stoller for reviewing the manuscript. This work was sponsored by the Office of Fusion Energy Sciences, U.S. Department of Energy, under contract DE-AC05-00OR22725 with UT-Battelle, LLC, and the “JUPITER-II” U.S. Department of Energy/Japanese Ministry of Education, Culture, Sports, Science, and Technology (MEXT) collaboration for fusion blanket and material systems research.

References

- [1] R. J. Price, Properties of silicon carbide for nuclear fuel particle coatings, *Nucl. Technol.* 35 (1977) 320–336.
- [2] N. P. Taylor, I. Cook, R. A. Forrest, C. B. A. Forty, W. E. Han, and D. J. Ward, The safety, environmental, and economic implications of the use of silicon carbide in fusion power plant blankets, *Fusion Eng. Des.* 58–59 (2001) 991–995.
- [3] B. Riccardi, L. Giancarli, A. Hasegawa, Y. Katoh, A. Kohyama, R. H. Jones, and L. L. Snead, Issues and advances in SiC_f/SiC composites development for fusion reactors, *J. Nucl. Mater.* 329–333 (2004) 56–65.
- [4] M. Abdou, D. Sze, C. Wong, M. Sawan, A. Ying, N. B. Morley, and S. Malang, U.S. plans and strategy for ITER blanket testing, *Fusion Sci. Technol.* 47 (2005) 475–487.
- [5] L. Giancarli, H. Golfier, S. Nishio, R. Raffray, C. Wong, and R. Yamada, Progress in blanket designs using SiC_f/SiC composites, *Fusion Eng. Des.* 61–62 (2002) 307–318.
- [6] R. Naslain, Design, preparation, and properties of non-oxide CMCs for application in engines and nuclear reactors: An overview, *Compos. Sci. Technol.* 64 (2004) 155–170.
- [7] L. L. Snead, M. C. Osborne, R. A. Lowden, J. Strizak, R. J. Shinavski, K. L. More, W. S. Eatherly, J. Bailey, and A. M. Williams, Low dose irradiation performance of SiC interphase SiC/SiC composites, *J. Nucl. Mater.* 253 (1998) 20–30.
- [8] T. Ishikawa, K. Bansaku, N. Watanabe, Y. Nomura, M. Shibuya, and T. Hirokawa, Experimental

- stress/strain behavior of SiC-matrix composites reinforced with Si-Ti-C-O fibers and estimation of matrix elastic modulus, *Compos. Sci. Technol.* 58 (1998) 51–63.
- [9] B. Schulz, Thermal conductivity of porous and highly porous materials, *High Temp. High Press.* 13 (1981) 649–660.
- [10] L. L. Snead, S. J. Zinkle, and D. P. White, Thermal conductivity degradation of ceramic materials due to low temperature, low dose neutron irradiation, *J. Nucl. Mater.* 340 (2005) 187–202.
- [11] Y. Katoh, T. Nozawa, and L. L. Snead, Mechanical properties of thin PyC interphase SiC-matrix composites reinforced with near-stoichiometric SiC fibers, *Journal of American Ceramic Society* (accepted).
- [12] Y. Katoh, T. Nozawa, L. L. Snead, T. Hinoki, A. Kohyama, N. Igawa, and T. Taguchi, Mechanical properties of chemically vapor-infiltrated silicon carbide structural composites with thin carbon interphases for fusion and advanced fission applications, *Mater. Trans.* 46 (2005) 527–535.
- [13] W. A. Curtin, Theory of mechanical properties of ceramic-matrix composites, *J. Am. Ceram. Soc.* 74 (1991) 2837–2845.
- [14] G. E. Youngblood, D. J. Senior, and R. H. Jones, Effects of irradiation and post-irradiation annealing on the thermal conductivity/diffusivity of monolithic SiC and f-SiC/SiC composites, *J. Nucl. Mater.* 329–333 (2004) 507–512.
- [15] L. L. Snead, Limits on irradiation-induced thermal conductivity and electrical resistivity in silicon carbide materials, *J. Nucl. Mater.* 329–333 (2004) 524–529.
- [16] L. L. Snead, M. Balden, R. A. Causey, and H. Atsumi, High thermal conductivity of graphite fiber silicon carbide composites for fusion reactor application, *J. Nucl. Mater.* 307–311 (2002) 1200–1204.
- [17] S. J. Zinkle and N. M. Ghoniem, Operating temperature windows for fusion reactor structural materials, *Fusion Eng. Des.* 51–52 (2000) 55–71.
- [18] K. Hironaka, T. Nozawa, T. Hinoki, N. Igawa, Y. Katoh, L. L. Snead, and A. Kohyama, High-temperature tensile strength of near-stoichiometric SiC/SiC composites, *J. Nucl. Mater.* 307–311 (2002) 1093–1097.